Chapter 2

Unidirectionally, Laterally Loaded Dowel-Type Fasteners Single-Bolt Joints

2.1 General

An analytical study of multiple-bolt joints should start with the review of the single fastener. Single-bolt joints under static loading have attracted much attention in the past and the subject is well researched, largely because it constitutes the simplest loading condition and joint configuration. Numerical and closed form stress models, especially for single-fastener joints, have come to a high level of complexity and versatility, particularly in the field of fiber-reinforced composite materials. This is not to say that the interaction of a single bolt with wood under static load is completely understood. Attributed to the non-uniformity of wood as a material, the complex failure mechanisms of bolt and wood, and varying material properties, the study of single-bolt joints in wood is likely to continue for some time to come.

This section attempts to compile and summarize, selected by subject, past findings and inductions that have contributed to the current understanding of the performance of single-bolt joints in timber. The discussion of multiple-bolt joints is deferred to Chapter 3.

2.2 Key Parameters Influencing Joint Behavior

2.2.1 Fastener Yield Strength

Slender fasteners, i.e. fasteners with high aspect ratios (length/diameter), typically bend when loaded in shear beyond the proportional limit. The plastic bending resistance of the fastener is referred to as its yield strength. Fastener yield strength substantially influences joint capacity containing slender fasteners, whereas it has no effect on joints with rigid dowels as the wood yields and fails before inelastic bending of the bolt takes place. Almost seven decades ago, Trayer (1932) noted that except for small aspect ratios, both fastener yield and wood strength control joint behavior. According to Trayer's tests, more rigid and less slender fasteners achieved higher proportional limit loads. Hence, recommended working stresses in design codes were initially lower for fasteners with higher aspect ratios.

Today, connection yield strength is related to wood crushing and bolt bending strength, and directly determines joint capacity and yield mode. The idea was first introduced by Johansen (1949) who linked the elastic bending capacity of the fastener to joint strength. In 1957 Meyer employed the full plastic bending capacity to determine joint strength, which is still used today (Figure 2.1).

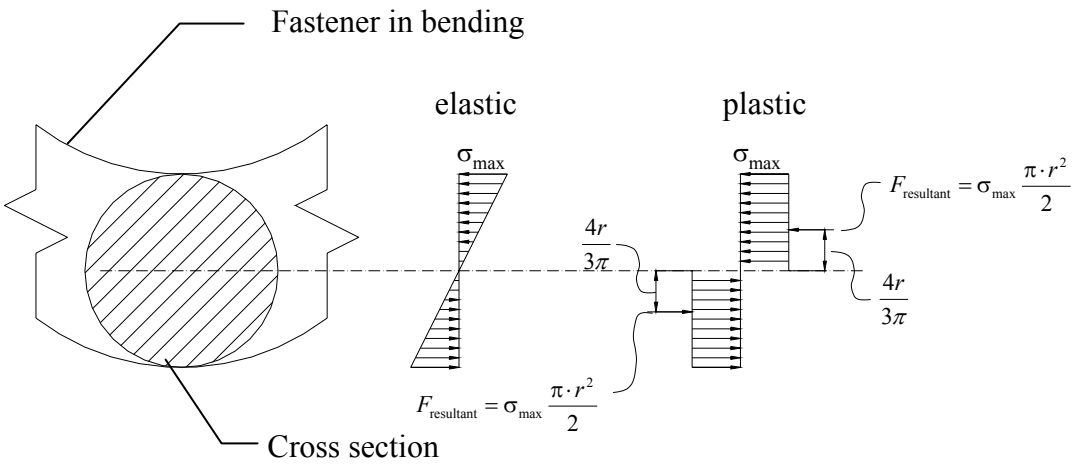

Figure 2.1: Illustration of elastic and plastic bending capacity of the fastener

Elastic bending moment:

$$M_{el} = \sigma_{\max,\text{elastic}} \cdot \frac{\pi \cdot d^3}{32} \tag{2.1}$$

Plastic bending moment:

$$M_{pl} = \sigma_{\max,\text{plastic}} \frac{2 \cdot \pi \cdot r^2}{2} \cdot \frac{4 \cdot r}{3 \cdot \pi} = \sigma_{\max} \cdot \frac{d^3}{6} \tag{2.2}$$

		Unit
M_{max}	maximum bending moment[1]	Nm
σ_{max}	bending stress or bending yield strength	N/m^2
d	fastener diameter	m
r	d/2	m
F	force resultant used to derive maximum moment	N

[1] Used in this work to describe both 5 percent offset moment and maximum moment.

Fastener yield strength is determined experimentally. In the U.S., the fastener is bent in three-point loading, and the load at 5 percent fastener diameter (used to compute M_{max}) is converted into bending yield strength using the equation

$$\sigma_{max} = \frac{6 \cdot M_{max}}{d^3} \tag{2.3}$$

In Europe, bending yield strength is also determined by Equation (2.3), but input parameters are acquired differently. Yield moment is defined as the smaller value of the maximum bending moment and the moment at a deformation of 45° under three-point loading. The methodology is less conservative than the U.S. approach, as the 5 percent offset bending yield strength falls in-between proportional limit strength and ultimate bending strength of the fastener. Harding and Fowkes (1984) originally suggested the 5 percent diameter offset load resulting in the adoption by the 1991 edition of the NDS. The main disadvantage of the offset approach is that it neither uses proportional limit nor capacity as a reference point. Moreover, attributed to joint settlement effects as loading commences, the fitting of an initial stiffness line is frequently ambiguous and judgmental. In addition, the offset approach is difficult to program if the analysis is conducted by a computer. A capacity based approach, on the other hand, exercised with appropriate adjustment factors to account for variability is relatively easy to program, clearly defined and promotes best material utilization.

Neither method accounts for strain hardening of the fastener. Due to hardening, the plastic bending resistance is not constant with increasing deformation. It follows that the plastic bending stress distribution is not uniform, resulting in altered fastener yield strength (Figure 2.2). For joints with slender dowels that undergo large deformations when loaded to failure, the true fastener yield strength is higher due to hardening. Mischler (1998) recommended that the true bending resistance of the dowel at the corresponding deformation be used as input in theoretical models.

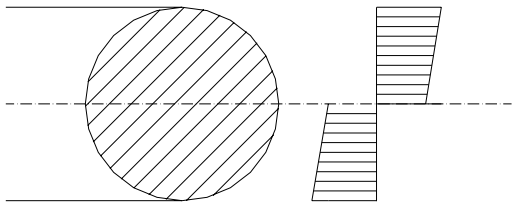

Figure 2.2: Bending stress distribution of fastener assumed to harden linearly

2.2.2 Dowel-Bearing Strength (Embedment Strength)

Dowel-bearing strength (or embedment strength) is a material property determined through testing that describes a limit stress state of the wood around a pin-loaded hole in compression. Until recently, dowel-bearing was determined in the U.S. using a specimen with a half hole containing a dowel uniformly loaded perpendicular to its axis in compression as outlined in ASTM D 5764 (ASTM 1995) (Figure 2.3). In Europe, dowel-bearing strength is obtained through a full-hole test as described in PrEN383 (1991) and also depicted in Figure 2.3. The problem with the half-hole test is that at lower fastener aspect ratios the wood beneath the fastener tends to split. Yet, in a joint the pin is loaded in a full hole where the surrounding wood provides some resistance to splitting. Consequently, the American Society of Testing and Materials reviewed the standard and now recommends the full-hole test for specimens with high tendency to split (ASTM 1998). The full-hole test has the disadvantage that, because of the way the fastener is loaded, it is almost impossible to avoid fastener bending, which implies the embedding stress is not constant over the whole length of the dowel.

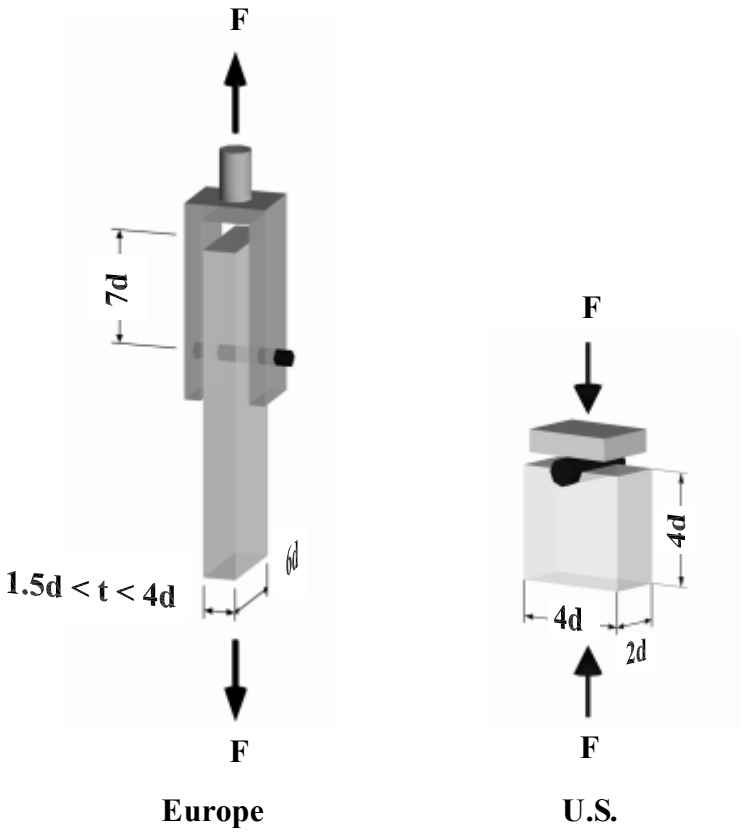

Figure 2.3: Embedment tests in Europe and the U.S.

Embedment strength is considerably influenced by loading direction (parallel or perpendicular to grain) not only because of a different modulus of elasticity of wood when compressed parallel or perpendicular to grain, but also on account of different failure modes (Gattesco 1998). Parallel to grain, embedment load increases almost linearly with increasing slip until sudden longitudinal splitting commences (Figure 2.4). The load drops somewhat, but increases further almost linearly with displacement, at close to zero slope, as longitudinal cracks grow and more wood gets crushed underneath the fastener. Perpendicular-to-grain embedment load-slip curves exhibit a much less distinct and much shorter linear portion as a result of the nonlinear compression characteristic of wood in that direction and due to the initiation of transverse splitting (Figure 2.4).

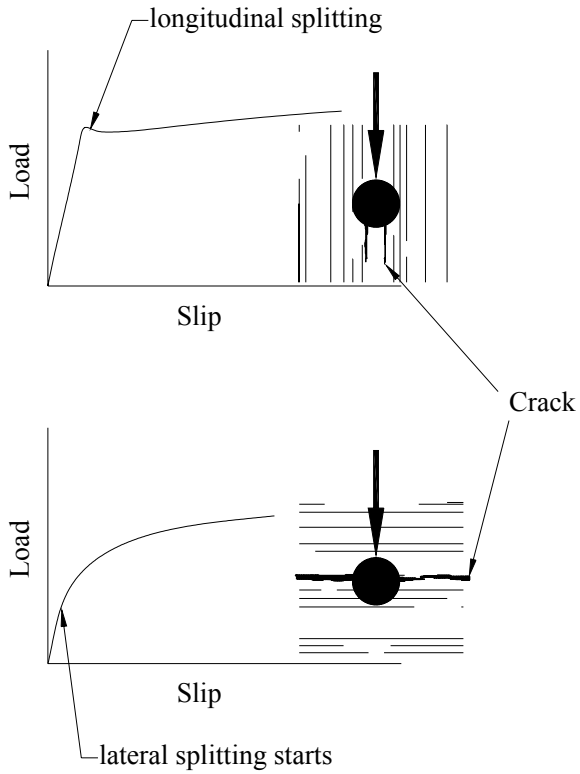

Figure 2.4: Typical load-slip curve of dowel embedment tests parallel and perpendicular to grain

Wilkinson (1991) derived the following empirical formulation relating bolt diameter and specific gravity to embedment strength for perpendicular and parallel to grain loading

$$\hat{F}_{e(parallel)} = 11{,}830 \cdot \hat{G}_{12} \tag{2.4}$$

$$\hat{F}_{e(perp)} = 6{,}620 \cdot \hat{G}_{12}^{1.45} \cdot \hat{d}^{-0.5} \tag{2.5}$$

		Unit
$\hat{F}_e$	embedment strength	psi
$\hat{d}$	fastener diameter	inch
$\hat{G}_{12}$	specific gravity based on ovendry weight and volume at 12 percent moisture content	
$\hat{G}$	specific gravity based on ovendry weight and volume	

The researcher did not find a significant effect of diameter on bearing strength parallel to the grain. Similar to fastener yield strength, embedment strength was determined as the load at 5 percent fastener diameter. In other words, Wilkinson derived Equations (2.4) and (2.5) based on the 5 percent offset load rather than capacity. Equations (2.4) and (2.5) include specific gravity based on ovendry weight and volume at 12 percent moisture content. Since specific gravity is more frequently reported at ovendry weight and volume, Equations (2.4) and (2.5) were changed to

$$\hat{F}_{e(parallel)} = 11{,}200 \cdot \hat{G} \tag{2.6}$$

$$\hat{F}_{e(perp)} = 6{,}100 \cdot \hat{G}^{1.45} \cdot \hat{d}^{-0.5} \tag{2.7}$$

and were adopted by the 1991 edition of the NDS. To convert the results of Equations (2.6) and (2.7) to metric units and timber density at 20°C/65% r.h., the following equations may be used.

$$F_{e(parallel)} = \hat{F}_{e(parallel)} \cdot 6.156 \cdot 10^{-6} \tag{2.8}$$

$$F_{e(perp)} = \hat{F}_{e(perp)} \cdot 1.31695 \cdot 10^{-6} \tag{2.9}$$

Earlier, Whale and Smith (1986) conducted embedment tests in an effort to provide an empirical formulation for the first draft of Eurocode 5. As opposed to Wilkinson, Whale and Smith found a significant influence of bolt diameter on embedment strength parallel to the grain.

$$F_e = \frac{0.082 \cdot (1 - 0.01 \cdot d) \cdot \rho_{12,12}}{k \cdot \sin^2 \alpha + \cos^2 \alpha} \tag{2.10}$$

Where, for hardwoods

$$k = 1.35 + 0.015 \cdot d \tag{2.11}$$

and softwoods

$$k = 0.9 + 0.015 \cdot d \tag{2.12}$$

		Unit
F_e	embedment strength	N/mm^2
$\hat{F}_e$	embedment strength	psi
d	fastener diameter	mm
$\hat{d}$	fastener diameter	inch
$\hat{G}_{12}$	specific gravity based on ovendry weight and volume at 12 percent moisture content	
$\hat{G}$	specific gravity based on ovendry weight and volume	
$\rho_{12,12}$	wood density based on weight and volume at 12 percent moisture content (20°C/65% R.H.)	Kg/m^3
α	angle between direction of load and direction of grain	°

Figures 2.5 and 2.6 portray European and converted US embedment strength models for the purpose of comparison. In general, as reflected by the graphs, embedment strength increases under fasteners with smaller diameter (except for Eqs. (2.8) and (2.9) where embedment strength is not influenced by diameter). This is attributed to the fact that for larger diameter fasteners splitting occurs due to perpendicular to grain tension stresses soon after proportional limit load is reached, and the fact that the embedment stress at proportional limit is not significantly different from the embedment stress at failure (Jorissen 1998). It is interesting to note that Whale and Smith obtained embedment strength at the maximum load in contrast to Wilkinson. Yet, for parallel to grain (except for small diameter bolts), the US model yields higher embedment strengths for a given species. Parallel to grain both models describe a linear relationship, whereas for perpendicular to grain, Wilkinson found an exponential correlation between fastener strength, bolt diameter and embedment strength as opposed to the European researchers, but did not find a significant difference between hardwoods and softwoods. Again, the fact that Wilkinson used the 5 percent offset load to determine embedment strength may explain why his model yields smaller values at larger fastener diameters, but gives larger values at smaller diameters when compared to the European model for softwoods. It should further be noted that Wilkinson used the half-hole test with uniform pressure application along the dowel as described above, while Whale and Smith assessed embedment strength employing the full-hole test, which was later included in European test standards. The full-hole tests produces both dowel bearing and dowel bending when small diameter fasteners are used.

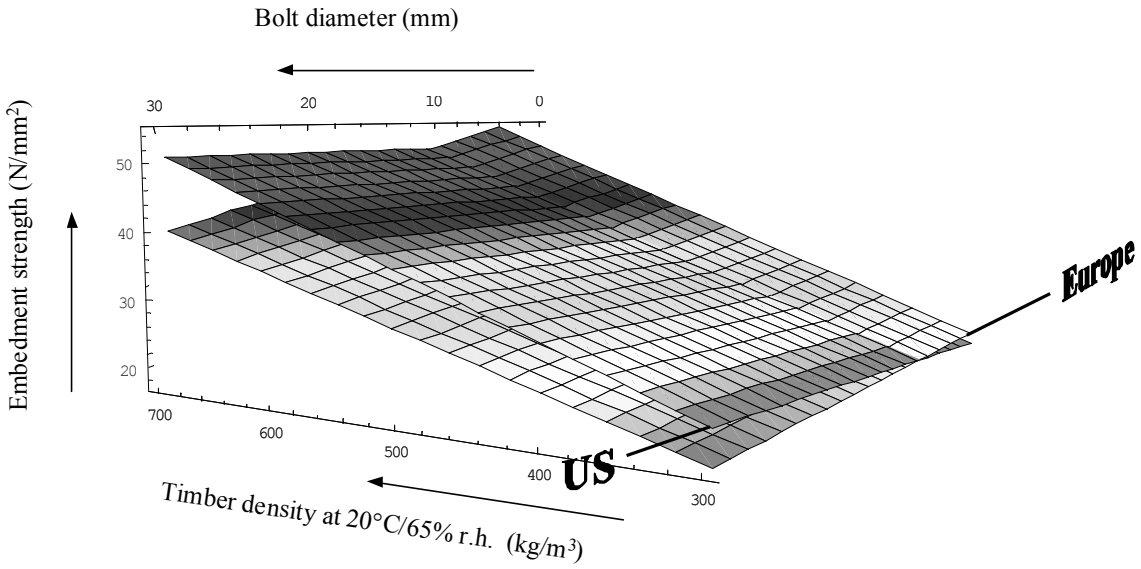

Figure 2.5: Embedment strength parallel to grain Europe versus US

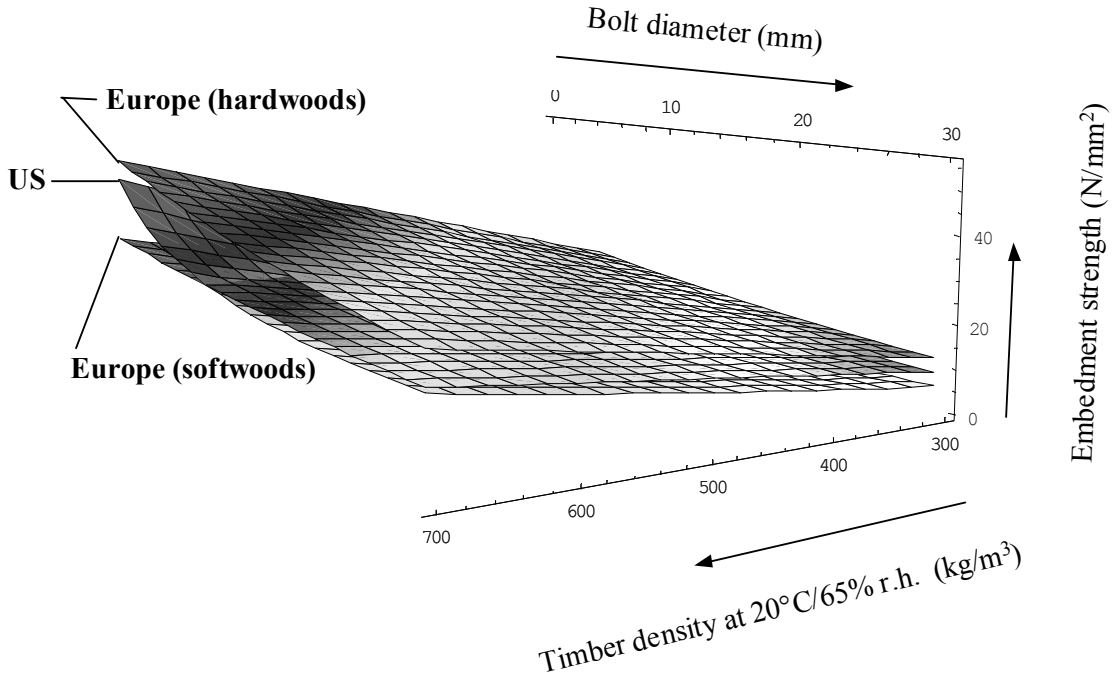

Figure 2.6: Embedment strength perpendicular to grain Europe versus US

2.2.3 Fastener Aspect Ratio

In the literature, fastener aspect ratio is frequently defined as the length of the fastener in the center member of a three-member joint divided by its diameter. Yet, in case of single shear joints this definition is not applicable. Therefore, fastener aspect ratio for this study is defined as

$$\lambda = \frac{t}{d} \tag{2.13}$$

where:

t = member thickness

d = fastener diameter

Obviously this definition implies that one obtains more than one aspect ratio for joints with different member thicknesses. Early research (Trayer 1932) identified that fastener aspect ratio is the principal factor determining bearing stress. It is well established that constant aspect ratio produces constant average bearing stress in wood as long as the fastener diameter does not fall within growth ring width.

Fastener aspect ratio determines to what degree fastener yield strength and embedment strength influence joint behavior. It controls the yield and failure modes of the joint. Joints containing rigid fasteners (small aspect ratios) tend to exhibit brittle failure modes on account of wood splitting, whereas slender fasteners bend and develop plastic hinges. At decreasing aspect ratios, more wood yielding and less fastener bending is involved. Figure 2.7 depicts the relation between proportional limit stress and fastener slenderness as found by Trayer (1932) who assumed uniform stress distribution beneath the bolt[2]. His tests on joints in double shear showed that for rigid fasteners with aspect ratios of λ smaller or equal to two, joint strength is fully governed by embedment strength as no appreciable bending of the fastener takes place. Hence, with no fastener bending involved, the proportional limit stress remains constant for changing aspect ratios, neglecting volumetric strength variations of wood.

[2] Trayer obtained the proportional limit stress by dividing the proportional limit load by the projected area of the fastener

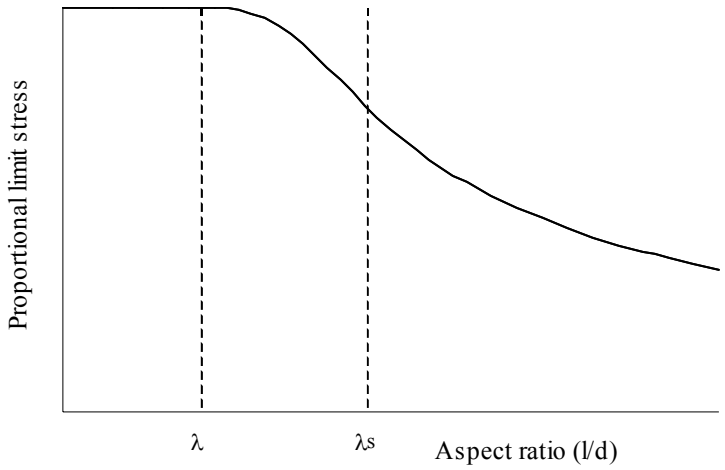

Figure 2.7: Proportional limit stress as a function of aspect ratio as determined by Trayer (1932)

Trayer observed that beyond the aspect ratio λ_s

$$\frac{\lambda_{n+1}}{\lambda_n} = \frac{\sigma_n}{\sigma_{n+1}} \tag{2.14}$$

The subscript 'n+1' denotes the next larger aspect ratio with the corresponding proportional limit stress. As a result, for fasteners with aspect ratio greater than λ_s the proportional limit load of the joint remains constant for a certain fastener diameter (Figure 2.7). This observation was later confirmed by Johansen's Yield Theory (Johansen 1949). In other words, Trayer discovered what is known today as Mode IV yield. For double shear connections Trayer determined λ_s to be about 5 ½.

2.2.4 Tensile or Compressive Loading

Because the members of a joint containing a single fastener are of finite dimension, the type of loading, tension or compression, influences capacity. The effect increases with decreasing edge distance. Studies of stress distributions around pin loaded holes have been mainly concerned with the magnitude and direction of stresses at the immediate pin/hole interface and have assumed that the medium around the fastener is of infinite dimension. Yet, stress distribution away from the hole is significantly influenced by the direction of loading in a finite member. Tensile loading causes the stress lines to run around the bolt resulting in tensile stresses

perpendicular to the grain, which promotes premature splitting of the timber. Capacity is therefore somewhat reduced for joints loaded in tension.

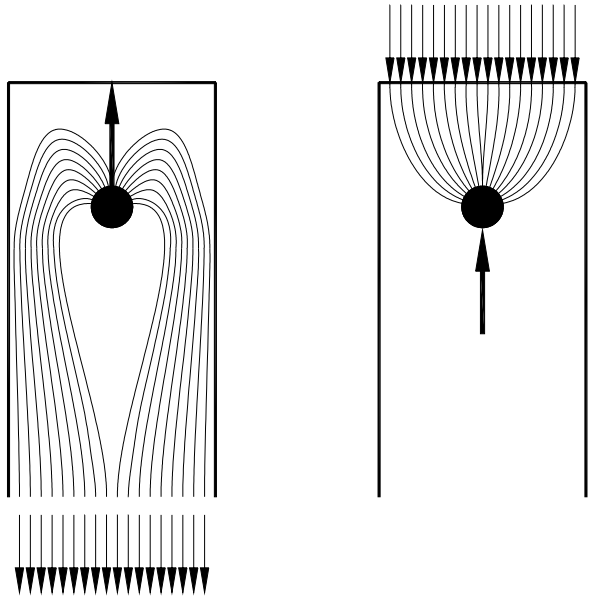

Figure 2.8: Stress lines due to tensile or compressive loading (after Jorissen 1998)

2.2.5 Friction

Bolted connections with nuts drawn tight develop significant friction between the abutting surfaces, which increases the capacity of the joint. Nonetheless, due to the rheological characteristics of wood, the compression force achieved by tightening the nuts is quickly lost. In addition, possible moisture related dimensional changes of the wood members turn surface friction between members into a rather variable element. As a result, some researchers have tested joints with bolts drawn fingertight or left loose (Trayer 1932, Johansen 1949). Considerable friction may, however, develop past the proportional limit when the bolts bend and draw the members against each other.

2.2.6 Fastener End Restraints

Very little experimental and analytical work has been done to investigate how fastener end fixity affects joint behavior. Effects of fixity of the bolt ends due to head, nut and washers depend on bolt diameter and side member material. X-ray scans carried out by Humphrey and Ostman (1989) on three member wood joints (side member thickness = 37.5 mm, main member thickness = 75 mm) containing a single bolt (∅ 12.5 mm) revealed that the thin steel side

members do not provide much resistance to bolt-end rotation despite the restraint imposed by head, nut and washers. However, analysis of test data reported in the literature by McLain and Thangjitham (1983) lead to the discovery that in single shear joints containing thicker side members (76 mm) bolt end fixities tend to reduce the likelihood of end rotation.

On the other hand, end fixity may introduce tensile forces in the bolt and may cause force components acting against the applied force (McLain and Thangjitham 1983). At higher displacements, the bolt or part of the bolt rotates and the inclined tensile force causes a force component in the direction of loading. Furthermore as a consequence of axial bolt tension, the normal force between the two joint members increases leading to a frictional force component in loading direction.

Since bolted joints must contain washers under head and nut by code regulation, the effects of end fixity should be included in any analytical or numerical model attempting to accurately replicate joint performance.

2.3 Basic Analytical Techniques

Numerous, often difficult to determine factors influencing bolt behavior make a generalization of bolted joint performance extremely complex. Analytical techniques have been developed to facilitate the formulation of mathematical prediction models.

2.3.1 Pin-Loaded Hole

Extensive research has been reported in the literature concerning pin-loaded holes in fiber-reinforced composite materials. Compared with wood, fiber reinforced composites show similar stress-strain characteristics in the elastic range when viewed in the principal material coordinate system. The modulus of elasticity (E) perpendicular to the fibers (E_2 or E_3) for a typical graphite polymer composite is approximately 8 percent of E parallel to the fibers (E_1) (Hyer 1997), which is also true for the average values of wood (Bodig and Jayne 1982). Hence, part of the discussion that follows is derived from research on composite materials.

2.3.1.1 Interface Friction and Crack Formation

Friction develops between fastener and hole boundaries when a joint is loaded perpendicular to the fastener axis. In general, interface friction influences the distribution of stresses around the hole to a magnitude sufficient to make it an important factor that should be included in every stress analysis of pin-loaded holes in orthotropic materials (Hyer et al. 1987). An influence on stresses around the hole implies possible effects on failure mechanism and

embedment strength. Rodd (1988) showed that interface friction indeed influences embedment strength in wood in a way that embedment strength decreases with decreasing interface friction. Figure 2.9 illustrates a pin-loaded hole with interface friction between fastener and wood. Friction causes crushing of fibers underneath the fastener rather than the bending of fibers around the bolt, which takes place at locations where friction is overcome (outside the compression region as shown in Figure 2.9). This triggers splitting at two locations underneath the bolt. The figure also exhibits the case where interface friction is reduced to zero and the splitting force, F_s, acting perpendicular to the grain, becomes significantly larger. From the foregoing, it can be concluded that a higher friction coefficient, μ, increases the compression region angle, ϕ, and the wood is less likely to split (Rodd 1988, Patton-Mallory 1996, Jorissen 1998). The smaller ϕ, the closer together the two cracks move, and the lateral displacement of the fibers is increased, which produces a higher wedging effect resulting in wood splitting at lower loads. At zero friction, only one crack would theoretically form in the center underneath the fastener.

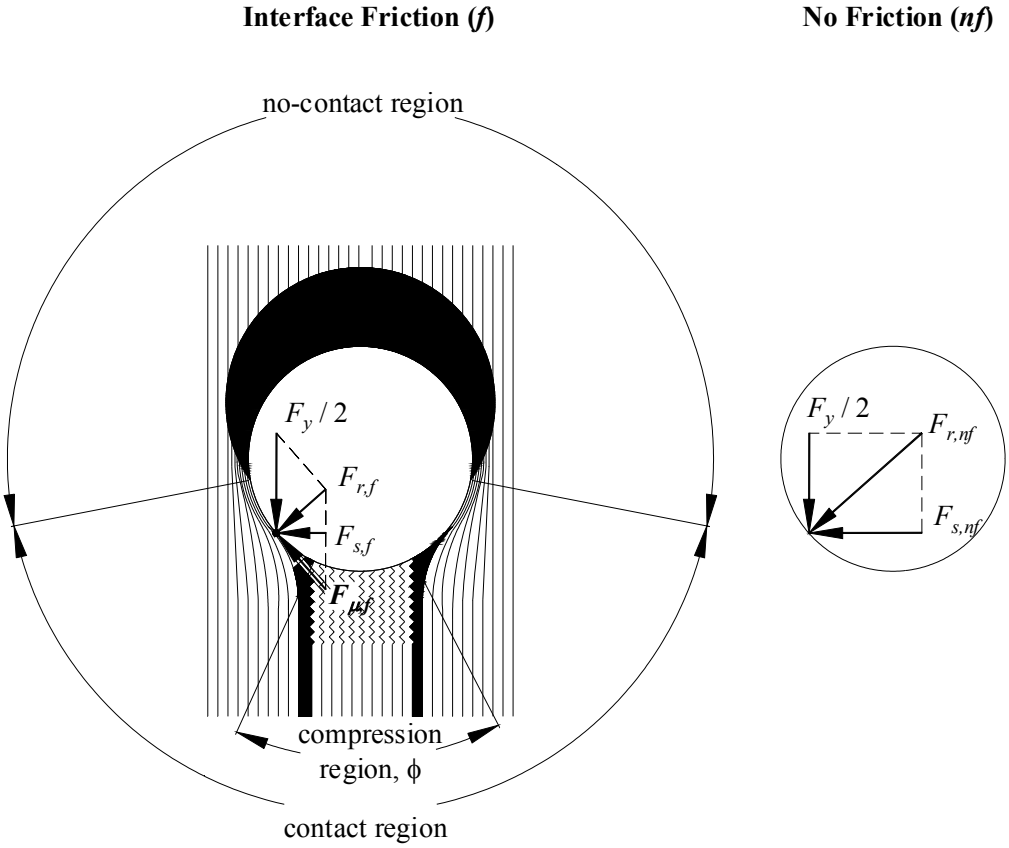

Figure 2.9: Influence of interface friction on crack formation. No friction (shown on right side) increases the splitting force F_s perpendicular to the grain.

Jorissen (1998) confirmed the formation of two cracks originating at the fastener hole through tests on double shear joints containing rigid bolts loaded parallel to the grain. He approximated the location of the cracks by assuming that crack formation commences at the point where the frictional force, F_μ, equals the tangential force component F_t, of the lateral force F_y (Figure 2.10).

$$2 \cdot b = d \cdot \sin\varphi \tag{2.15}$$

		Units
F_y	lateral force	N
F_t	tangential force component	N
F_μ	frictional force	N
d	fastener diameter	mm
φ	angle of friction	degrees

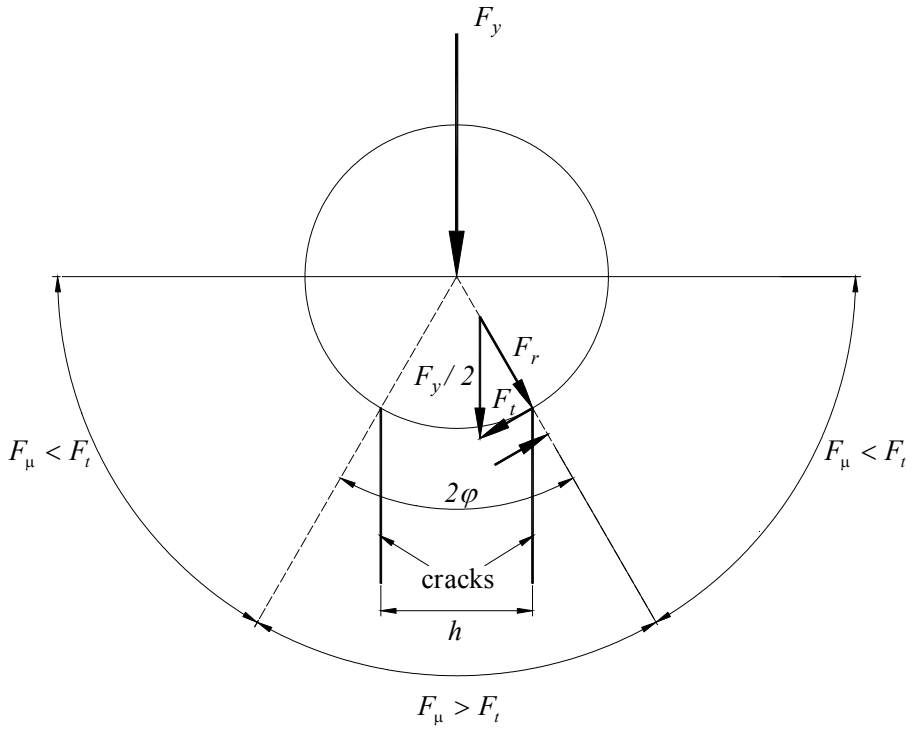

Figure 2.10: Crack location according to Jorissen (1998). Crack commences where $F_\tau = F_\mu$.

2.3.1.2 Clearance

Fastener-hole clearance not only influences the overall stress magnitude around the hole, but also affects the location and direction of stress maxima, because it decreases the contact region and increases stress concentration (Hyer et al. 1987, Eriksson 1986). Furthermore, it is suspected that hole clearance explains some of the uneven load distribution observed on multiple bolt joints.

2.3.1.3 Stress Distribution

Knowledge of stress distributions is essential to predict failure accurately. Yet, the true stress distribution around a pin-loaded hole in orthotropic materials is very complex. Under the assumption of plain stress, the analytical derivation to determine the true stress distribution in an orthotropic plate containing a hole, loaded in tension or compression was established by Lekhnitskii (1968). His intricate functions have been incorporated into many theoretical works. The approximate stress distribution along the two principal axes of a pin-loaded plate with no clearance is shown in Figure 2.11. As a result of stress concentrations at the hole boundary, in the directions perpendicular and parallel to the load, stresses parallel to the grain decrease rapidly with increasing distance to the hole, both in transverse and longitudinal direction.

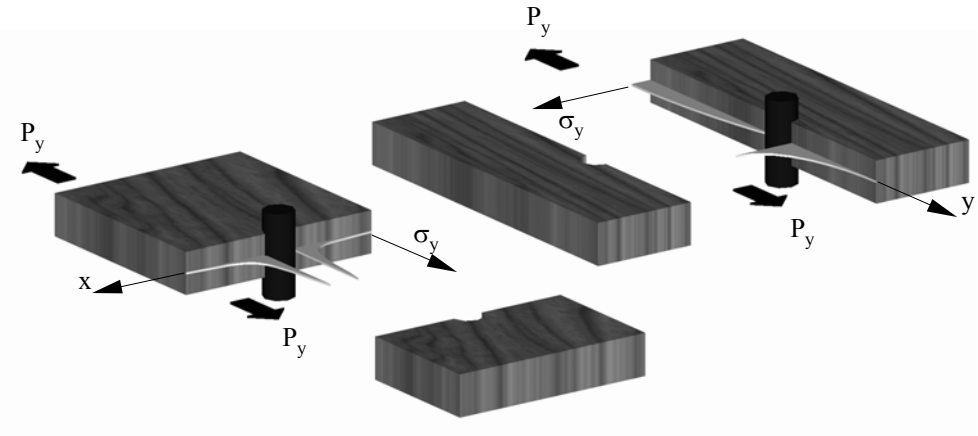

Figure 2.11: Stress distribution along the x-and y-axis of a pin-loaded plate.

A major contribution was made by de Jong (1977, 1982) who derived stress distributions around a pin-loaded hole in an infinite orthotropic plate based on Lekhnitskii's work. De Jong's late works include the effects of friction, but assume a rigid pin and no initial clearance between pin and hole. A good synopsis of the calculations was given by Ireman et al. (1993). For further information, the reader is referred to Ireman et al. (1993), de Jong (1977/82), and Lekhnitskii (1968).

In 1977, De Jong presented the stress distribution parallel and perpendicular to the fibers around a pin-loaded hole in a unidirectional composite plate whose behavior in the elastic region would be similar to a wooden plate. The analysis precluded friction, and a tight fit was assumed. On grounds that stress concentrations next to a hole reduce quickly with increasing distance, De Jong attempted to approximate a joint of finite width but infinite length by superposition of two loading scenarios (Figure 2.12). Based on these simplifications, De Jong presented stress distributions (normalized based on average bearing stress) in the principal x-and y-directions of a unidirectional carbon fiber reinforced plate of finite width but infinite length (Figure 2.13 'No Friction'). The results can be extended to a wooden plate containing an infinitely rigid dowel, which is loaded in the elastic range and moves in the y-direction only (Mode I).

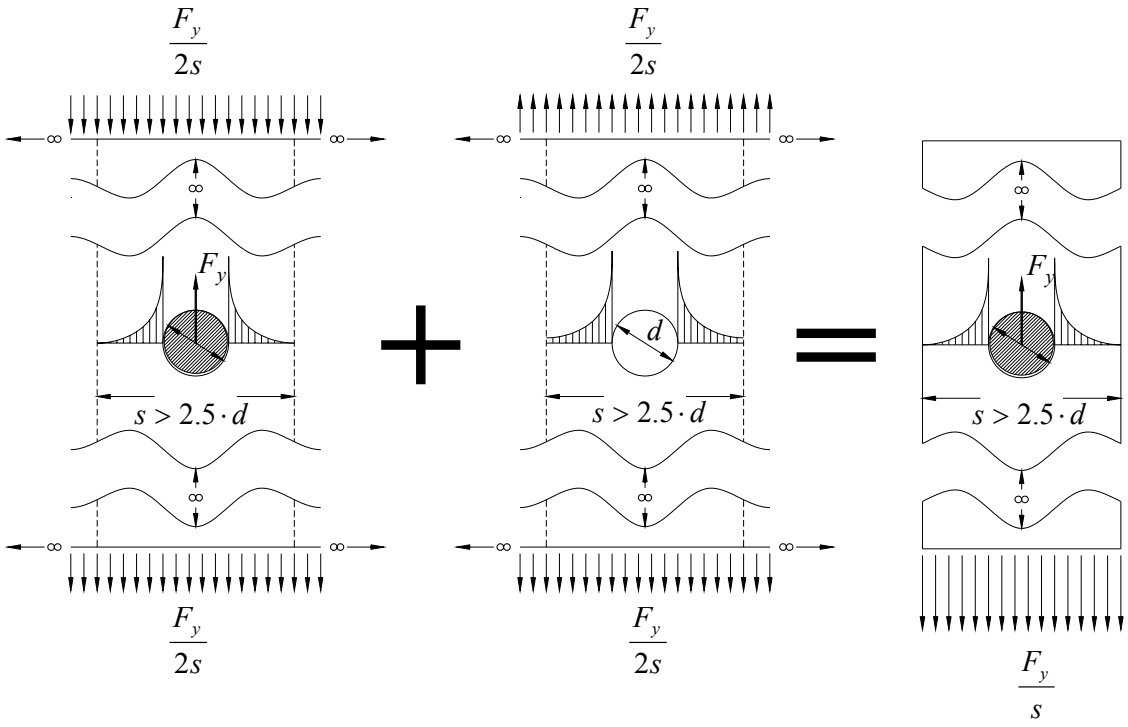

Figure 2.12: Approximation for a plate with finite width through superposition of two loading scenarios in infinite plates (after De Jong 1977).

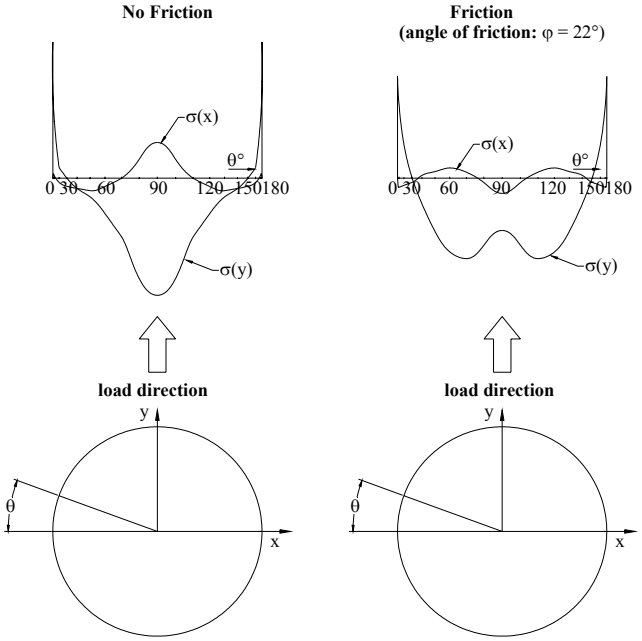

Figure 2.13: Stress distribution around a pin loaded hole in a uni-directional carbon fiber laminate (after De Jong 1977)

Figure 2.13 also reveals the approximate stress distribution around a pin-loaded hole with an assumed angle of friction of 22°. The graph was devised by the author of this document for a unidirectional laminate based on past data of a $(90_4/\pm45)_s$ laminate (De Jong 1982). The general effect of friction on the stress distribution can be observed. The maximum bearing stress σ_y is reduced and occurs away from $\theta = 90°$. In addition, when friction is considered, the stress perpendicular to the grain, σ_x, is compressive at $\theta = 90°$ in contrast to it being a tensile stress when friction is not accounted for. Moreover, interface friction produces a shear stress along the hole edge (not shown in the figure). The locations of the tension maxima of σ_x both with and without interface friction explains the crack formation around rigid doweled joints as elaborated in the previous section.

2.3.1.4 Stress Concentration Factor

The stress state around the perimeter of a small circular hole in an infinite, homogeneous plate of radius *r* under uniaxial tension is given by (Boresi et al. 1993)

$$\sigma_\theta = \sigma(1 - 2\cos 2\theta) \tag{2.16}$$

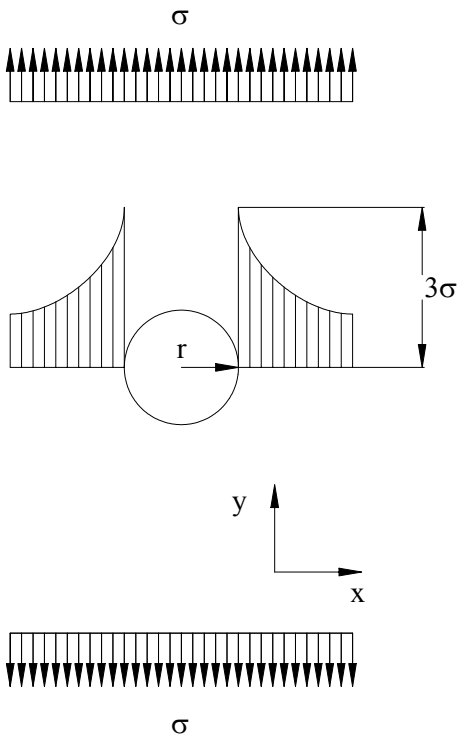

Figure 2.14: Localized stress concentration in an infinite plate containing a hole under uniaxial tension

Equation (2.16) assumes its maximum value of $\sigma_{\theta(max)} = 3\sigma$ for $\theta = \pi/2$ and $\theta = 3\pi/2$. Thus, the stress concentration factor at a circular hole in an infinite plate loaded in tension equals 3. Equation (2.16)'s applicability to plates with finite width is limited to circular holes with diameters considerably smaller than the width of the plate. In summary of previous work, Boresi et al. (1993) gave the following formula to determine the stress concentration factor for loaded plates with finite width containing a large diameter hole compared to the width of the plate

$$S_c = \frac{\sigma_{max}}{\sigma_n} = \frac{3 \cdot \kappa - 1}{\kappa + 0.3} \tag{2.17}$$

		Units
θ	angle between positive y-axis and point on perimeter of hole	
S_c	stress concentration factor	
σ_n	Average stress over cross sectional area excluding the hole	N/m^2
κ	Ratio of plate width to hole diameter	

2.3.1.5 Comments

While these studies are extremely useful because they present a closed-form solution and give some insight about stress distributions and failure modes, their application to timber joints is limited. Only Mode I-type deformations in the elastic range can be approximated with this approach, as other deformation modes would violate the plain-stress assumption. Furthermore, contemporary design practices for timber joints allow for plastic deformation of the joint. Yet, exact stress prediction beyond the elastic limit is extremely complex without numerical approximation.

2.3.2 Beam on Elastic Foundation

A dowel-type fastener embedded in wood and laterally loaded is akin to a beam on an elastic foundation. Studies of beams on elastic foundations have been reported in the literature for more than a century. Early interest on this subject was sparked by the railroad industry that studied rail response. General analyses have focused on beams on a linear elastic Winkler foundation, first introduced by E. Winkler (1867). In a Winkler foundation, the reaction forces are proportional to the beam deflection at any point. It is assumed that the foundation is not capable of transferring shear forces. In other words, the foundation can be modeled as an infinite number of independent springs supporting the beam. In addition, the Winkler hypothesis assumes that the foundation acts both in tension and compression. Hence, the beam is always in contact with the foundation and does not lift off.

According to Hetényi (1946), the deflection curve of a beam on a Winkler foundation between concentrated transverse loading forces can be described by the differential equation

$$E \cdot I \cdot \frac{d^4 y}{dx^4} = \frac{d^2 M}{dx^2} = \frac{dQ}{dx} = -k \cdot y \tag{2.18}$$

with the general solution

$$y = e^{\lambda \cdot x}\left(C_1 \cdot \cos(\lambda \cdot x) + C_2 \cdot \sin(\lambda \cdot x)\right) + e^{-\lambda \cdot x}\left(C_3 \cdot \cos(\lambda \cdot x) + C_4 \cdot \sin(\lambda \cdot x)\right) \tag{2.19}$$

where

$$\lambda = \left(\frac{k}{4 \cdot E \cdot I}\right)^{\frac{1}{4}} \tag{2.20}$$

The integration constants are determined based on boundary conditions.

		Units
E	modulus of elasticity beam material	N/m^2
I	moment of inertia	m^4
k	modulus of foundation per beam width	N/m^2
x	distance from origin of coordinates	m
y	beam deflection (orthogonal to x)	m
C_i	integration constant	
λ	characteristic of the system	1/m

Using the Winkler-foundation assumption, Bhat and Xirouchakis (1986) found an exact solution for the deflection profile of an elastic-plastic floating beam subjected to concentrated load at midlength up to and beyond the formation of a three-plastic-hinge failure mechanism. The beam was assumed to be perfectly elastic plastic with an ideal I-section. Furthermore, beam deflections were considered small compared to the beam depth to comply with the simple beam theory.

The application of the theory of beams on elastic foundation to wood joints has been frequently reported in the literature. Most research employed the Winkler foundation model in an attempt to fit a linear elastic load-slip relation. Yet, modern design methodologies shifted from using linear elastic approximations to non-linear elastic-plastic analysis. This is in part attributed to the fact that the application of the Winkler foundation model to wood gives moderate predictions at best. Wood is not linear elastic when stressed to capacity and the analysis of joints requires a look beyond the elastic limit. The European Yield theory (Johansen 1949), utilizes a beam on a *plastic* foundation approach by holding onto the assumption that at capacity wood crushing underneath the fastener is so advanced that the reaction force is uniformly distributed along the fastener and the wood foundation is assumed to be perfectly plastic. While simplifying the problem to a great extent and being capable of predicting joint capacity, the European Yield Theory fails to relate capacity or any other loading state to joint slip. A more detailed discussion of the Yield Theory is covered in a later section.

Foschi (1974) used a beam on an elastic-plastic foundation approach to derive a finite element model capable of predicting the load-slip function of laterally loaded nails in wood. Rather than using the linear elastic Winkler foundation, Foschi exploited a non-elastic foundation model to account for crushing of the wood underneath the nail. The characteristics of the foundation were expressed as

$$p = \left(P_0 + P_1 x\right) \cdot \left(1 - e^{\frac{-k \cdot x}{P_0}} \right) \tag{2.21}$$

		Unit
p	reaction force of foundation	N
k	initial stiffness	N/mm
P_1	slope of the asymptote	N/mm
P_0	y-intercept	N
x	displacement	mm

For perfect yield (wood crushing at constant load), $P_1 = 0$ and Equation (2.21) equals the load slip relation reported more than four decades earlier by Teichmann and Brokmann (1930 and 1931). The constants k, P_1 and P_0 can be acquired from nonlinear least squares fitting of experimental data obtained through embedment tests (Figure 2.15). Foschi's model has been used by many researchers (Dolan 1989, White 1995, Blass 1994, Frenette 1997) as input for comprehensive finite element analyses and empirical joint models.

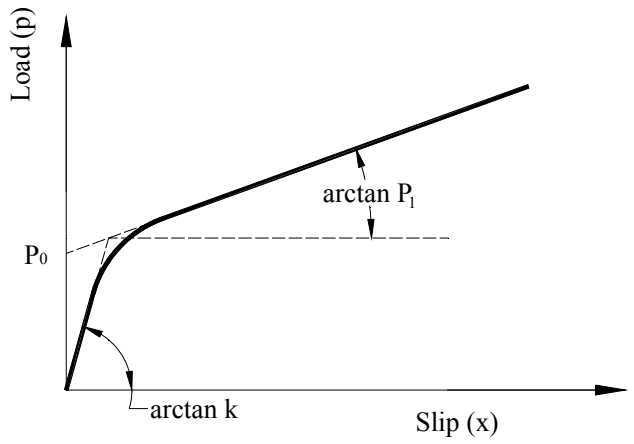

Figure 2.15: Foundation model (Foschi 1974)

2.3.2.1 Comments

After a comprehensive review of previous work, Smith (1983) concluded that beam on foundation joint models give adequate prediction of capacity and yield load, given tight fit of the connector and load is applied parallel to the grain. Predictability is less certain for load directions perpendicular to the grain.

2.4 Prediction Models

In light of ever-increasing computing power, the capabilities of structural analysis today have become enormous. Numerical modeling has become powerful enough to provide approximated solutions with great accuracy of the most complex problems. Yet, the accuracy of

numerical and analytical models rises and falls with the ability to quantify pertinent material properties and their interactions which provide crucial information on material and connection behavior that influence wood systems (Bodig et al. 1991).

There is an abundance of connection models reported in the literature. It is not the purpose of this study to provide a complete description of all formulations attempting to predict joint behavior.

2.4.1 The European Yield Model

The European Yield Model laid the foundation for a sound engineering approach to joint design. Because its application is so widespread today, the European Yield Theory deserves special attention.

It has taken more than four decades for global acceptance of the European Yield Model first developed by the Danish scientist Johansen (1949) and later refined and expanded by Möller (1950) and Meyer (1957). The model predicts lateral yield strength of a connection containing a single dowel-type fastener, such as a bolt or nail, based on bending resistance of the fastener and the crushing strength of wood. The model is limited to predicting a limit state load. Fastener dimensions and yield strength, dowel bearing strength and thickness of the connection members determine the governing yield mode. Aune and Patton-Mallory (1986), McLain and Thangjitham (1983), and Soltis et al. (1986) established the applicability of the European Yield Theory to nails and bolts in wood, leading to an adoption of the yield equation by the 1991 edition of the National Design Specification (NDS) in the United States.

The model assumes that both fastener bending and wood strain are perfectly plastic at limit state, without accounting for joint behavior prior to limit state. Accordingly, as indicated in Figure 2.16, the true load-slip curve is replaced by plastic function A in Europe and B in the United States. However, as discussed in Section 2.1.2.2, due to dissimilar empirical equations and methods to derive them, the spread between the two empirically determined functions of the embedment load-slip curves may be larger or smaller (or even negative) depending on fastener diameter and loading direction.

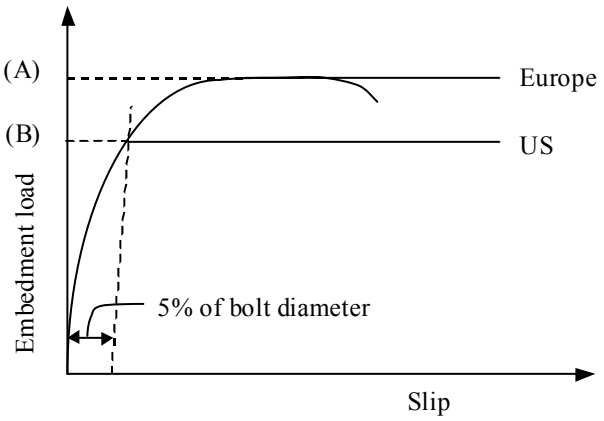

Figure 2.16: Plastic embedment load-slip behavior as determined in the US and Europe.

In order to simplify the derivation, Johansen considered only perfectly symmetric two and three member joints, all of which had approximately equal bearing strength. For single shear joints, the scientist observed and analytically described two different yield modes. Figure 2.17 illustrates the basic concept of the model using a single shear joint under the first yield mode described by Johansen. The derivation of lateral joint capacity using conditions of equilibrium is based on the assumption that at capacity the joint behaves perfectly plastic with a uniform stress distribution along the wood-to-fastener contact area equaling the wood bearing strength.

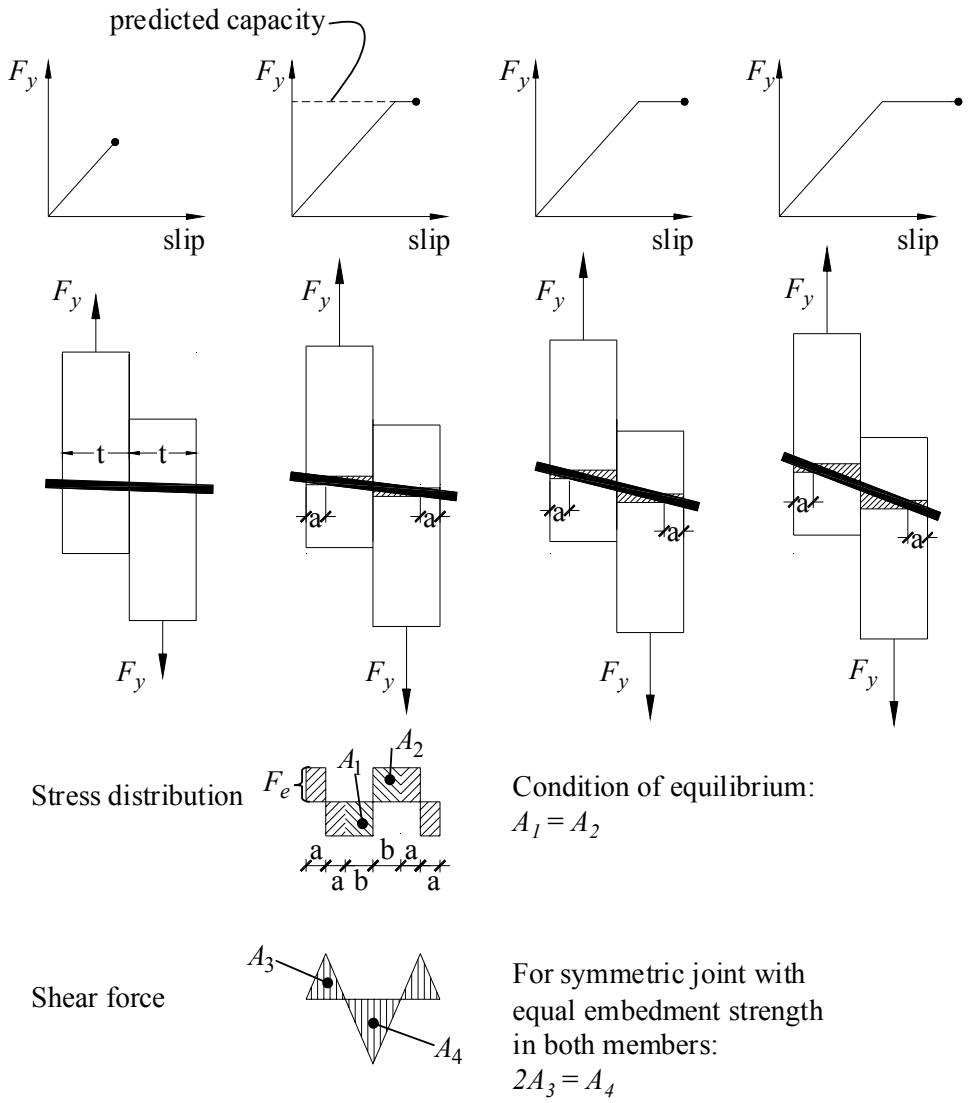

Figure 2.17: Johansen's Model. At capacity, wood crushing underneath the fastener is so advanced that the reaction force is uniformly distributed along the fastener and constant relative to joint slip (moments and forces caused by asymmetry are not shown).

The yield model in use today analytically identifies four basic yield modes for fasteners in single shear as depicted in Figures 2.18 through 2.21[3]. The numbering of the yield modes follows that of the NDS (1991), while the accompanying equations are based on a publication by Hilson (1995) and do not include any safety factors unlike the formulations published in the NDS.

[3] Note that forces and moments due to asymmetry are assumed to be absorbed by the surrounding structure and are not shown in the figures.

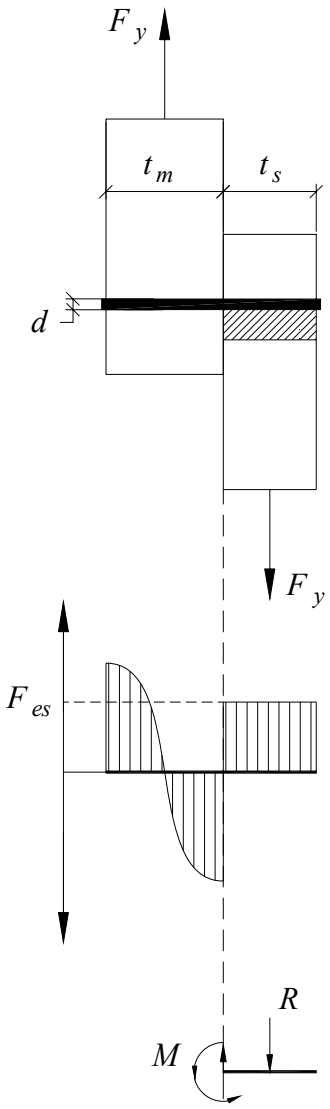

Figure 2.18: Mode 1 yield

For yield in the side member we can write

$$F_y = R = F_{es} \cdot t_s \cdot d \tag{2.22}$$

However, if yield occurs in the main member we find

$$F_y = F_{em} \cdot t_m \cdot d \tag{2.23}$$

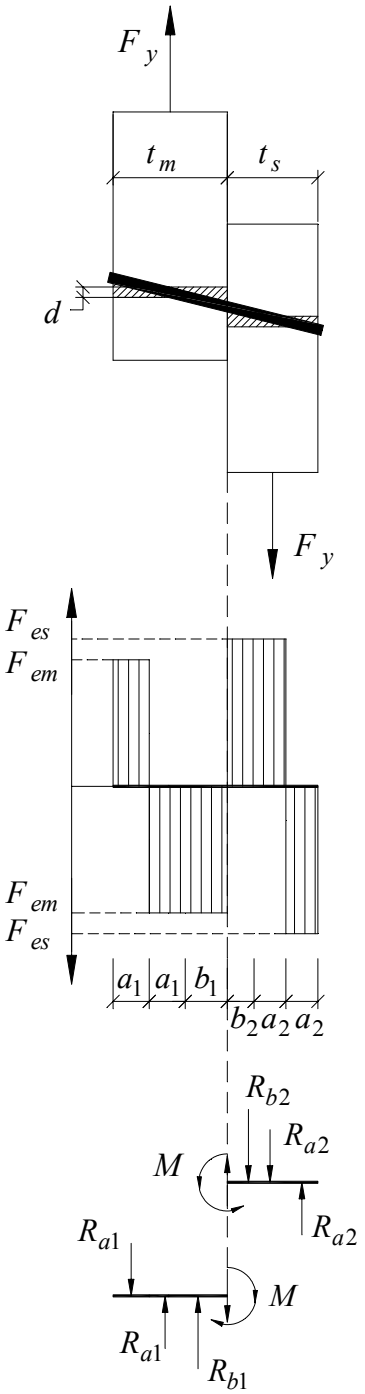

Figure 2.19: Mode II yield

Since yield occurs in both members, the joint force may be expressed as

$$F_y = F_{em} \cdot b_1 \cdot d = F_{es} \cdot b_2 \cdot d \tag{2.24}$$

If (Figure 2.19)

$$M = R_{a1} \cdot \left(b_1 + a_1 + \frac{1}{2} \cdot a_1 \right) - R_{a1} \cdot \left(b_1 + \frac{1}{2} \cdot a_1 \right) - R_{b1} \frac{1}{2} \cdot b_1 \tag{2.25}$$

then

$$M = F_{em} \cdot d \cdot \left(a_1^2 - \frac{b_1^2}{2} \right) = F_{es} \cdot d \cdot \left(\frac{b_2^2}{2} - a_2^2 \right) \tag{2.26}$$

Using the following relations

$$b_2 = b_1 \cdot \frac{F_{em}}{F_{es}} \qquad \text{(to satisfy equilibrium)} \tag{2.27}$$

$$a_1 = \frac{t_m - b_1}{2} \tag{2.28}$$

$$a_2 = \frac{t_s - b_2}{2} = \frac{\frac{F_{es}}{F_{em}} t_s - b_1}{2 \frac{F_{es}}{F_{em}}} \tag{2.29}$$

And substituting Equations (2.28) and (2.29) into Equation (2.25) and solving for b_1 gives

$$b_1 = \frac{t_m}{1+\frac{F_{es}}{F_{em}}} \cdot \left[\sqrt{\frac{F_{es}}{F_{em}} + 2 \cdot \left(\frac{F_{es}}{F_{em}}\right)^2 \left[1 + \frac{ts}{t_m} + \left(\frac{ts}{t_m}\right)^2 \right] + \left(\frac{F_{es}}{F_{em}}\right)^3 \cdot \left(\frac{ts}{t_m}\right)^2} - \frac{F_{es}}{F_{em}} \cdot \left(1 + \frac{ts}{t_m}\right) \right] \tag{2.30}$$

Finally, substitution of b_1 in Equation (2.24) yields

$$F_y = d \cdot F_{em} \frac{t_m}{1+\frac{F_{es}}{F_{em}}} \cdot \left[\sqrt{\frac{F_{es}}{F_{em}} + 2 \cdot \left(\frac{F_{es}}{F_{em}}\right)^2 \cdot \left[1 + \frac{t_s}{t_m} + \left(\frac{t_s}{t_m}\right)^2 \right] + \left(\frac{F_{es}}{F_{em}}\right)^3 \cdot \left(\frac{t_s}{t_m}\right)^2} - \frac{F_{es}}{F_{em}} \cdot \left(1 + \frac{t_s}{t_m}\right) \right] \tag{2.31}$$

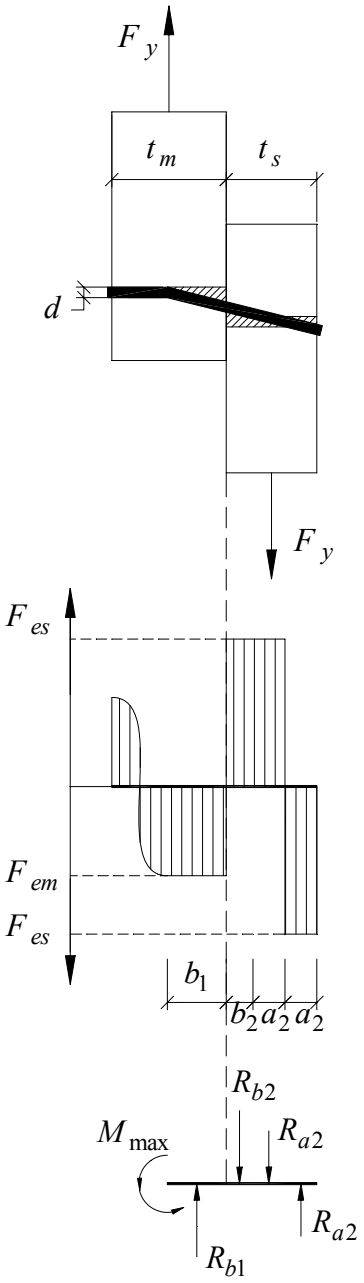

Figure 2.20: Mode III yield

No matter where the plastic hinge occurs, we can write

$$F_y = F_{em} \cdot b_1 \cdot d = F_{es} \cdot b_2 \cdot d \tag{2.32}$$

The maximum moment occurs at the plastic hinge where shear force is zero. Thus

$$M_{\max} = -R_{b1} \cdot \frac{b_1}{2} + R_{b2} \cdot \left(b_1 + \frac{b_2}{2} \right) + R_{a2} \cdot \left(b_1 + b_2 + \frac{a_2}{2} \right) - R_{a2} \cdot \left(b_1 + b_2 + \frac{3}{2} a_2 \right) \tag{2.33}$$

or

$$M_{\max} = -F_{em} \cdot d \cdot \frac{b_1^2}{2} + F_{es} \cdot d \cdot b_2 \left(b_1 + \frac{b_2}{2} \right) + F_{es} \cdot d \cdot a_2 \cdot \left(\left(b_1 + b_2 + \frac{a_2}{2} \right) - \left(b_1 + b_2 + \frac{3}{2} a_2 \right) \right) \tag{2.34}$$

Replacing b_1 by Equation (2.27), using Equations (2.28) and (2.29) in terms of b_2, and solving for b_2 yields

$$b_2 = \frac{-t_s}{2 \cdot \frac{F_{es}}{F_{em}} + 1} + \sqrt{\frac{t_s^2}{\left(2 \cdot \frac{F_{es}}{F_{em}} + 1 \right)^2} + \frac{t_s^2}{2 \cdot \frac{F_{es}}{F_{em}} + 1} + \frac{4 \cdot M_{\max}}{F_{es} \cdot d \cdot \left(2 \frac{F_{es}}{F_{em}} + 1 \right)}} \tag{2.35}$$

Finally, substitution of b_2 in Equation (2.32) with Equation (2.35) changes the expression of F_y to

$$F_y = \frac{-t_s \cdot F_{es} \cdot d}{2 \cdot \frac{F_{es}}{F_{em}} + 1} + F_{es} \cdot d \sqrt{\frac{t_s^2}{\left(2 \cdot \frac{F_{es}}{F_{em}} + 1 \right)^2} + \frac{t_s^2}{2 \cdot \frac{F_{es}}{F_{em}} + 1} + \frac{4 \cdot M_{\max}}{F_{es} \cdot d \cdot \left(2 \cdot \frac{F_{es}}{F_{em}} + 1 \right)}} \tag{2.36}$$

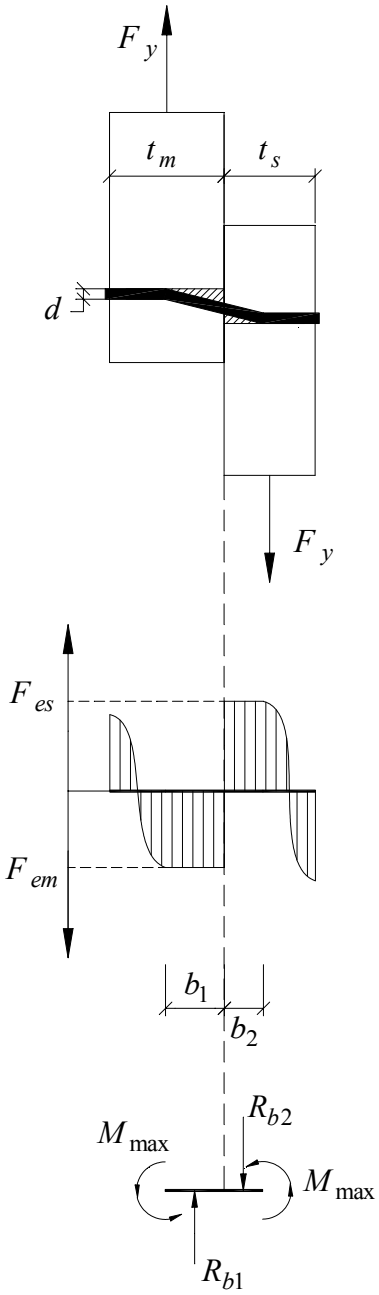

Figure 2.21: Mode IV yield

As with the other yield modes, the basic F_y of Mode IV may be expressed as

$$F_y = F_{em} \cdot b_1 \cdot d = F_{es} \cdot b_2 \cdot d \tag{2.37}$$

Again, the maximum moment occurs at plastic hinge where shear force is zero. Then

$$2 \cdot M_{\max} = -R_{b1} \cdot \frac{b_1}{2} + R_{b2} \cdot \left(b_1 + \frac{b_2}{2} \right) \tag{2.38}$$

or

$$2 \cdot M_{\max} = -F_{em} \cdot d \cdot \frac{b_1^2}{2} + F_{es} \cdot d \cdot b_2 \cdot \left(b_1 + \frac{b_2}{2} \right) \tag{2.39}$$

Replacing b_2 by Equation (2.27) and solving for b_1 produces

$$b_1 = \frac{2 \cdot \sqrt{M_{\max}}}{\sqrt{F_{em} \cdot d \cdot \left(1 + \frac{F_{em}}{F_{es}} \right)}} \tag{2.40}$$

Hence

$$F_y = 2 \cdot F_{em} \cdot d \sqrt{\frac{M_{\max}}{F_{em} \cdot d \cdot \left(1 + \frac{F_{em}}{F_{es}} \right)}} \tag{2.41}$$

		Unit
F_y	joint force	N
F_{em}	embedment strength of main member	N/mm^2
F_{es}	embedment strength of side member	N/mm^2
d	fastener diameter	mm
M_{max}	maximum bending moment of fastener	Nmm
R	force resultant	N
t_m	thickness of main member	mm
t_s	thickness of side member	mm

2.4.2 The Yield Model – What It is and What It is Not

Previously, NDS specifications for connections were based on empirical formulations, and due to the need for interpretation, the section had grown considerably since the first edition. With adoption of an equation format, a significant breakthrough towards an engineering mechanics approach for the design of dowel-type connections was accomplished. Single fastener joint design is now on a firm mechanics foundation and is less ambiguous and confounding (McLain 1991). Although the theory tends to give somewhat conservative results because when the bolt deforms, part of the tensile load is in loading direction, the applicability and predictability of the theory for single-bolt joints with slender fasteners has been confirmed by a number of researchers (McLain and Thangjitham 1983; Soltis et al. 1986; Wilkinson 1992). Predictions by the model seem to agree more closely to experimental data of parallel to the grain loaded joints than to joints subjected to perpendicular-to-grain loading (Soltis and Wilkinson 1987). Compared to other analytical formulations, the European Yield Model entails closed-form and rather simple equations that are easily solved using contemporary spreadsheet software.

Despite its popularity, the European Yield Model has some shortcomings. Obviously the model does not predict deformations attributed to any loading state. Hence, any displacement related properties such as stiffness, ductility, or energy dissipation cannot be determined using the yield model. Furthermore, the Yield Theory implies that fastener aspect ratio is the principal factor for the normalized joint bearing strength (Soltis et al. 1986). Thus, bearing strength found for a smaller diameter bolt could predict the strength for a larger diameter bolt if the aspect ratio remains the same. However, this is only true assuming that no brittle failure such as splitting, plug shear, or tensile failure in the reduced cross section occurs. For stiff bolts with small aspect ratios, predicted joint capacities are frequently higher than observed by experiments, as the connection tends to split before plastic deformation takes place.

Patton Mallory (1986) noted that because of the high variability of embedment strength, yield strengths of failure modes depending more on embedment strength (i.e. fasteners with small aspect ratios) generally show higher variability than strengths which are more dependent on fastener bending. In addition, the European Yield Model does not account for oversized holes or friction between joint members.